PASJ: Publ. Astron. Soc. Japan **65**, S4, 2013 December 5

Relations between Strong High-Frequency Microwave Bursts and Proton Events

Victor V. GRECHNEV,[1] Nataliya S. MESHALKINA,[1] Ilya M. CHERTOK,[2] and Valentin I. KISELEV[1]
[1]*Institute of Solar-Terrestrial Physics SB RAS, Lermontov St. 126A, Irkutsk 664033, Russia*
grechnev@iszf.irk.ru
[2]*Pushkov Institute of Terrestrial Magnetism, Ionosphere and Radio Wave Propagation (IZMIRAN), Troitsk, Moscow, 142190 Russia*
ichertok@izmiran.ru

(Received 2013 April 8; accepted 2013 July 30)

Abstract

Proceeding from close association between solar eruptions, flares, shock waves, and CMEs, we analyze relations between bursts at 35 GHz recorded with the Nobeyama Radio Polarimeters during 1990–2012, on the one hand, and solar energetic particle (SEP) events, on the other hand. Most west to moderately east solar events with strong bursts at 35 GHz produced near-Earth proton enhancements of $J(E > 100\,\mathrm{MeV}) > 1$ pfu. The strongest and hardest of those caused ground-level enhancements. There is a general, although scattered, correspondence between proton enhancements and peak fluxes at 35 GHz, especially pronounced if the 35 GHz flux exceeds 10^4 sfu and the microwave peak frequency is high. These properties indicate emission from numerous high-energy electrons in very strong magnetic fields suggesting a high rate of energy release in the flare–CME formation process. Flaring above the sunspot umbrae appears to be typical of such events. Irrespective of the origin of SEPs, these circumstances demonstrate significant diagnostic potential of high-frequency microwave bursts and sunspot-associated flares for space weather forecasting. Strong prolonged bursts at 35 GHz promptly alert to hazardous SEP events with hard spectra. A few exceptional events with moderate bursts at 35 GHz and strong proton fluxes look challenging, and should be investigated.

Key words: proton events — Sun: flares — Sun: radio radiation

1. Introduction

Solar energetic particles (SEP), which are somehow accelerated in association with solar eruptive events, offer hazards for equipment and astronauts on spacecraft, and even for passengers and crew members on aircraft in high-latitude flights due to secondary particles. The highest-energy extremity of SEP events sometimes produces in the Earth's atmosphere considerable fluxes of secondary neutrons, which are able to cause ground-level enhancements (GLE) of the cosmic-ray intensity registered preferentially with high-latitude neutron monitors (see, e.g., Cliver 2006; Aschwanden 2012; Nitta et al. 2012). The lowest latitude, at which a GLE is observed, is determined by the energy of primary particles.

The existing methods to diagnose SEP productivity of a solar eruption, which has just occurred, are not yet perfect. Still larger uncertainties exist in forecasting SEP events. An elaboration of existing methods calls for a better understanding of particle acceleration, when and where it occurs, and in which conditions.

SEPs mainly consist of protons, alpha particles, and heavier ions. Their energies range from tens to hundreds of MeV, and sometimes up to several GeV. Unlike electrons, which are widely manifest in all layers of the solar atmosphere, practically in the whole observable range of electromagnetic emissions, starting from the gamma-ray bremsstrahlung continuum and up to metric radio waves, energetic protons on the Sun can only be detected from gamma-ray emissions appearing in their interactions with dense material (see, e.g., Vilmer et al. 2011). These are discrete gamma-ray lines in a range of 0.5–10 MeV produced by nuclei with energies of a few tens of MeV, and a very broad line at around 70 MeV produced in the decay of neutral pions, which appear in the interactions of protons with energies exceeding 300 MeV. The π^0-decay emission can only be identified with high-sensitivity gamma-ray spectrometers in big flares, and therefore the number of all events, in which this emission has been detected so far, starting from its first observation reported by Forrest et al. (1986), is as small as one dozen (see Chupp & Ryan 2009; Kurt et al. 2013; Vilmer et al. 2011 for the review; recent case studies, e.g., by Grechnev et al. 2008; Kuznetsov et al. 2011; Ackermann et al. 2012). Imaging in nuclear gamma-ray lines is only possible from data of Reuven Ramaty High-Energy Solar Spectroscopic Imager (RHESSI: Lin et al. 2002), and does not exceed the energy of the 2.22 MeV line. One more source of information about accelerated particles on the Sun is provided by solar neutrons, which are produced in collisions of high-energy protons, and are sometimes registered with low-latitude neutron monitors on the sunlit side of Earth (e.g., Watanabe et al. 2003; Vilmer et al. 2011) as well as some space-borne detectors.

It is possible to follow propagation in the interplanetary space of energetic electrons from their signatures in decameter to kilometer radio waves. On the other hand, the lack of observations, which could track heavy energetic particles from the Sun to Earth, hampers our understanding their origin. There are two different major viewpoints concerning on the origins of SEPs in interplanetary space (see, e.g., Kallenrode 2003; Grechnev et al. 2008; Reames 2013 and references therein). One concept relates SEPs with flare processes within an active region (e.g., Klein & Trottet 2001; Aschwanden 2012).

According to a different concept, SEPs are accelerated to high energies by a bow shock driven by the outer surface of a super-Alfvénic CME (e.g., Cliver et al. 1982; Reames 1999, 2009, 2013; Gopalswamy et al. 2012). The seemingly incompatibility of the two concepts is due to the traditional idea that particle acceleration occurs either (i) within a closed flaring solar active region or (ii) rather far from the Sun by a shock wave, whose properties are determined by the CME, and not by the flare. The CME and flare are considered to be independent of each other.

On the other hand, studies during the last years, supported by increasing observational material, specify long-standing issues and update corresponding concepts. The CME acceleration turns out to be closely associated with a flare, and occurs simultaneously with HXR and microwave bursts (Zhang et al. 2001; Temmer et al. 2008, 2010; Grechnev et al. 2011a). The helical component of the CME's magnetic flux rope responsible for its acceleration is formed by reconnection, which is also responsible for a flare (Qiu et al. 2007; Temmer et al. 2010). There is a detailed quantitative correspondence between the reconnected flux and the rate of energy release during a flare (e.g., Miklenic et al. 2009). Thus, the parameters of a CME should correlate with the parameters of the associated flare. This has been established indeed (e.g., Vršnak et al. 2005).

Furthermore, Grechnev et al. (2011a, 2011b) and Afanasyev and Uralov (2011) have shown that shock waves, most likely, are excited by erupting flux ropes as impulsive pistons inside developing CMEs, and this occurs during hard X-ray and microwave flare bursts (i.e., at the rise phase of the soft X-ray emission). Then, the shock wave detaches from the piston, and quasi-freely propagates afterwards like a decelerating blast wave. The transition of the shock wave to the bow-shock regime is expected in a typical situation later. As the results of Reames (2009) show, the release of SEPs near the Sun occurs within a few solar radii. The parameters of the shocks at such distances should be mainly determined by their initial sources, and therefore related to the parameters of the associated flares. Also note that from the preceding paragraph it follows that the early evolution of the CME speed is expected to be roughly proportional to the soft X-ray flux time profile at the rising phase. That is, if the soft X-ray flux increases gradually, then the development of a shock wave is not expected at small distances from the Sun.

CMEs should favor the escape of flare-accelerated particles trapped in the flux rope (K.-L. Klein 2011 private communication). Reconnection of the expanding CME's flux rope with a coronal streamer allows trapped particles to access magnetic fields, which are open into interplanetary space, and facilitates their escape, thus solving the problem discussed by Cliver et al. (1989). A possible extremity is presented by jet-like eruptions, when reconnection decomposes the magnetic flux rope (e.g., Meshalkina et al. 2009).

These considerations show that the traditional contrasting of the flare-acceleration and shock-acceleration options is probably exaggerated. There are convincing arguments in favor of either option. While gamma-rays nearly concurrent with different flare emissions favor flare-acceleration of heavy particles simultaneously with electrons, there is no reason to object to shock-acceleration, if in situ measurements of the SEP composition, such as the iron charge state, Fe/O ratio, and other parameters, indicate the acceleration of ions at normal coronal temperatures (see, e.g., Reames 2009, 2013). On the other hand, in situ measurements are limited to moderate energies of ions, while the acceleration of heavier particles is more efficient by Fermi processes operating in shock-acceleration, indeed. It is possible that the contesting concepts are based on different observations subjected to selection effects.

For all these reasons, it seems to be logical to expect a correspondence between parameters of SEPs and microwave bursts. Indeed, the correlation between SEP events and strong high-frequency radio bursts has been known for many decades (e.g., Croom 1971). On the other hand, Kahler (1982) explained this association by the 'Big Flare Syndrome,' i.e., a general correspondence between the energy release in an eruptive flare and its various manifestations, whereas the actual SEP acceleration was considered to be by a CME-driven bow shock. Later exaggerations of the shock-acceleration concept have led to an underestimation of the diagnostic opportunities of microwave bursts. However, it seems worth to analyze the relations between flare microwave bursts and SEPs irrespective of their origins. Some aspects of the correspondence between the parameters of flares, CMEs, shock waves, and SEPs have been really stated by Nitta et al. (2003) and Gopalswamy et al. (2012).

The relations between SEP events and microwave bursts at 9 GHz were considered by Akinian et al. (1978) and Cliver et al. (1989). This frequency can belong to either an optically thin or thick branch of the gyrosynchrotron spectrum. This complicates the relation. Higher-frequency emissions in the optically thin regime seem to be the most sensitive to large numbers of high-energy electrons gyrating in strong magnetic fields, being thus directly related to the rate of energy release in the flare–CME formation process. The frequency of 35 GHz is the highest one, at which stable long-term observations are available, thanks to the operation of the Nobeyama Radio Polarimeters (NoRP: Nakajima et al. 1985). In the present study, we analyzed the relations between microwave bursts recorded with NoRP since 1990, on the one hand, and large high-energy proton enhancements, on the other hand. Systematic lists are available of data on proton events (e.g., Kurt et al. 2004; Chertok et al. 2009) and especially on GLE events (e.g., Cliver 2006).

Chertok et al. (2009) found that the $F_{35} > 10^4$ sfu criterion selected SEP-productive events, and not only west ones. We extend our analysis to a larger set of events with $F_{35} > 10^3$ sfu occurring during the NoRP observational daytime. To reveal the events missed by our criterion, we also considered all near-Earth > 100 MeV proton enhancements exceeding $J_{100} > 10$ pfu [1 pfu $= 1$ particle cm^{-2} s^{-1} ster^{-1}], whose solar source events could be observed in Nobeyama.

The input data, their processing, and the output parameters are considered in section 2. Section 3 analyzes the parameters of near-Earth proton enhancements versus the parameters of microwave bursts estimated in section 2. Besides the proton-rich events associated with intense bursts at 35 GHz, seven additional events have been revealed from the lists of SEP events by the $J_{100} > 10$ pfu criterion. Three of these SEP enhancements were due to solar backside events, whose

microwave emissions were occulted. The 35 GHz fluxes for four remaining exceptional proton-rich events ranged from 140 to 780 sfu. Section 4 shows that a proton-productive event can be expected if a related flare occurs in strong magnetic fields, especially in those associated with sunspots; discusses possible reasons for the exceptional events; and proposes a tentative relation between the peak flux observed at 35 GHz and the expected importance of a SEP event. Section 5 briefly summarizes the outcome of our analysis.

2. Data

2.1. Processing of NoRP Records

Data on solar microwave bursts recorded with NoRP are automatically processed by software, and posted on the NoRP web site. The results are sometimes insufficiently accurate, e.g., in evaluation of the pre-burst level, and can suffer from various problems. These circumstances required an examination of all records in question, and an evaluation of the parameters in the interactive mode.

NoRP records at 35 GHz for some events were absent or damaged. In such cases, the value of F_{35} was estimated by means of interpolation from the 17 GHz and 80 GHz data. The 80 GHz fluxes during 1995–2005 were corrected with a time-dependent factor of $[T_{\rm year}/1995.83]^{630}$ (H. Nakajima 2005 private communication). The NoRP did not operate at both 35 GHz and 80 GHz on 2004 November 10; the parameters of this event were roughly estimated from lower-frequency data and correlation plots of the Nobeyama Radioheliograph (NoRH: Nakajima et al. 1994). We had to deal with the 2001 April 21 event[1] in a similar way.

The turnover frequency, $f_{\rm peak}$, of the microwave spectrum was computed from the NoRP total flux data by using a parabolic fit of the averaged log–log spectrum near the peak of the burst. This method was previously used by White et al. (2003) and Grechnev et al. (2008). Here, we used data of lower-frequency polarimeters, which were located before 1994 in Toyokawa (Torii et al. 1979).

The time profiles of the bursts at 35 GHz are sometimes complex, contain more than one peak, etc. They are typically shorter and more impulsive than those at lower microwaves, and are quite different from soft X-ray ones, whose time profiles are intrinsically gradual. It is difficult to measure the duration of a burst at 35 GHz, Δt_{35}, with a simple formal criterion, e.g., by referring to 0.5 or to 0.1 and 0.9 levels. We have not yet found an adequate formal criterion to characterize durations of complex bursts, and therefore estimated Δt_{35} manually by marking characteristic durations. These estimates are rather subjective, and need elaboration. Nevertheless, they represent a general tendency correctly. The tendency remains, if the formal 0.5-level criterion is used, while the durations, Δt_{35}, become shorter.

2.2. Data Table

For convenience, we categorize the events according to their microwave fluxes, and denote the groups similar to the GOES class: mX (microwave-eXtreme) with $F_{35} > 10^4$ sfu, mS (microwave-Strong) with 10^3 sfu $< F_{35} < 10^4$ sfu, mM (microwave-Moderate) with 10^2 sfu $< F_{35} < 10^3$ sfu, and mO (microwave-Occulted).

The events and evaluated parameters of the bursts at 35 GHz along with data on near-Earth protons are presented in table 1. It lists chronologically the four groups of events in the descending order of their microwave importance, i.e., mX, mS, mM, and mO.

Column 1 of table 1 presents the event number in the table in the form No^{Q}. The superscript, Q, specifies the qualifier of the event, defined as follows:

Q0 – East event, no CME, no type II burst;

Q2 – West event with a CME and a type II burst;

Q1 – For all other events.

The qualifiers are only indicated for those events that could be observed by SOHO/LASCO, according to the SOHO LASCO CME catalog (Yashiro et al. 2004).[2]

Columns 2 and 3 indicate the date and time of the flare peak according to GOES reports. Columns 4, 5, and 6 present the GOES and Hα importance of the flare and its coordinates.

Columns 7, 8, and 9 present the burst duration, the maximum flux at 35 GHz in thousands of sfu (1 sfu $= 10^{-22}$ W m^{-2} Hz^{-1}), and the microwave peak frequency.

Columns 10 and 11 list the maximum near-Earth total fluxes of protons with $E > 100$ MeV (J_{100}) and with $E > 10$ MeV (J_{10}). Column 12 characterizes the integral proton spectrum with a parameter, $\delta_{\rm p} = \log_{10}(J_{10}/J_{100})$, which is calculated from the peak fluxes of protons with different energies occurring at different times, thus attempting to take account of their velocity dispersion. Column 13 presents the magnitude of a GLE, if it has occurred.

3. Results

3.1. General Outcome

Table 1 demonstrates that most mX events produced SEP events, indeed: 89% of both west and east mX events (total 19) produced proton enhancements, with $J_{100} > 1$ pfu for 68% of the 19 events. Considerable proton fluxes were observed after those events with very strong bursts at 35 GHz, even with their rather far-east location. A reduced proton productivity had two west events, Nos. 4 and 5, after which enhancements were distinct for > 10 MeV protons only. About 30% of the mX events produced GLEs. In these events, the proton spectrum indices were $\delta_{\rm p} < 2$, and the microwave peak frequencies $f_{\rm peak} \geq 18$ GHz (32 GHz on average over the 19 events).

The proton productivity of mS events is considerably lower. None of them produced a GLE. Totally, 52% of the mS events (both west and east) were not followed by any detectable enhancement, even of > 10 MeV protons.

To make the results clearer, figure 1 presents the data from Table 1 as peak proton fluxes with $E > 100$ MeV vs. peak microwave fluxes at 35 GHz. The events without detectable proton fluxes falling outside the region of the plot are presented at the horizontal dotted line, corresponding to 10^{-2} pfu to show their amount. A total of 18 west events and 29 east events have not produced detectable SEP fluxes. Similarly, three backside

[1] These two events are shown in figure 1 with the filled squares.

[2] ⟨http://cdaw.gsfc.nasa.gov/CME_list⟩.

Table 1. Analyzed events.

No.[Q]*	Date	$T_{\rm peak}$	Flare			Microwave burst				Protons near Earth		
			GOES	Hα	Position	Δt_{35} (min)	$F_{\rm max}$ (10^3 sfu)	$f_{\rm peak}$ (GHz)	J_{100} (pfu)	J_{10} (pfu)	$\delta_{\rm p}$	GLE (%)
1	2	3	4	5	6	7	8	9	10	11	12	13
mX events with extreme fluxes at 35 GHz ($F_{35} > 10^4$ sfu)												
1	1990-04-15	02:59	X1.4	2B	N32E54	66	20	11	0.04	9	2.4[‖]	—
2	1990-05-21	22:15	X5.5	2B	N34W37	7	38	47	18	300	1.22	24
3	1991-03-22	22:44	X9.4	3B	S26E28	2	122	35	55	28000	2.70	—
4	1991-03-29	06:45	X2.4	3B	S28W60	7	11	30	<0.1	20	—	—
5	1991-05-18	05:13	X2.8	2N	N32W87	26	21	26	<0.1	7	—	—
6	1991-06-04	03:41	X12	3B	N30E60	15	130[†]	44	2	50	1.40	—
7	1991-06-06	01:09	X12	3B	N33E44	17	130[†]	46	2.5	200	1.90	—
8	1991-06-09	01:39	X10	3B	N34E04	7	74	36	1.2	80	1.82	—
9	1991-06-11	02:06	X12	3B	N32W15	18	46	30	42	2500	1.77	12
10	1991-10-24	02:38	X2.1	3B	S15E60	0.6	34	35	—	—	—	—
11	1992-11-02	02:54	X9	2B	S23W90	15	41	35	70	800	1.06	6.5
12[2]	2001-04-02	21:48	X17	—[‖]	N18W82	6	25	35	4.8	380	1.90	—
13[0]	2002-07-23	00:31	X4.8	2B	S13E72	17	15	35	—	—	—	—
14[2]	2002-08-24	01:00	X3.1	1F	S02W81	16	11	18	27	220	0.91	14
15[2]	2004-11-10	02:10	X2.5	3B	N09W49	7	>10[‡,§]	>17[‡,§]	2	75	1.57	—
16[2]	2005-01-20	06:46	X7.1	2B	N12W58	25	85	28	680	1800	0.42	5400
17[2]	2006-12-13	02:40	X3.4	4B	S06W24	31	14	45	88	695	0.89	92
18[1]	2012-03-07	00:24	X5.4	3B	N17E15	80	11	17	67	1500	1.35	—
19[2]	2012-07-06	23:08	X1.1	—[‖]	S15W63	3	17	35	0.27	22	1.91	—
mS events with strong fluxes at 35 GHz ($10^3 < F_{35} < 10^4$ sfu)												
20	1990-05-11	05:42	X2.4	SF	N15E13	14	2.0	15	—	—	—	—
21	1990-05-21	01:24	M4.8	1B	N33W30	7	1.3	31	—	—	—	—
22	1990-05-23	04:20	M8.7	1B	N33W55	10	1.0	10	—	—	—	—
23	1990-06-10	07:17	M2.3	2B	N10W10	3	1.0	19	—	—	—	—
24	1991-01-25	06:32	X10	1N	S12E90	6	9.4	28	0.3	1	0.52	—
25	1991-03-05	23:26	M6.2	SF	S23E79	2	1.4	11	—	—	—	—
26	1991-03-07	07:49	X5.5	3B	S20E62	3	2.0	32	—	—	—	—
27	1991-03-13	08:03	X1.3	2B	S11E43	2	3.6	15	0.03	4.6	2.18	—
28	1991-03-16	00:48	X1.8	2B	S10E09	3	3.2	28	—	—	—	—
29	1991-03-16	21:52	M6.0	2B	S09W04	4	1.6	21	—	—	—	—
30	1991-03-19	01:57	M6.7	2B	S10W33	1	7.2	32	—	—	—	—
31	1991-03-21	23:39	M5.4	2B	S25E40	3	7.2	32	—	—	—	—
32	1991-03-23	22:06	M5.6	2B	S25E16	15	1.7	29	—	—	—	—
33	1991-03-25	00:17	X1.1	2B	S26E01	11	3.9	18	—	—	—	—
34	1991-03-25	08:09	X5.3	3B	S25W03	4	4.2	18	0.5	150	2.47	—
35	1991-05-16	06:49	M8.9	2B	N30W56	9	8.0	27	—	—	—	—
36	1991-05-29	23:43	X1.0	2B	N05E38	1	1.7	21	—	0.8	—	—
37	1991-06-30	02:56	M5.0	1N	S06W19	0.8	2.0	20	0.2	—	—	—
38	1991-07-30	07:07	M7.2	1N	N14W58	0.9	2.0	30	—	—	—	—
39	1991-07-31	00:48	X2.3	2B	S17E11	5	1.6	18	—	—	—	—
40	1991-08-02	03:13	X1.5	2B	N25E15	8	1.2	13	0.15	—	—	—
41	1991-08-03	01:22	M2.9	1N	N24E05	3	2.8	25	0.15	—	—	—
42	1991-08-25	00:51	X2.1	2B	N24E77	29	1.4	10	0.03	21	2.84	—
43	1991-10-27	05:42	X6.1	3B	S13E15	6	8.8	12	—	40	—	—
44	1991-11-02	06:45	M9.1	2B	S13W61	3	1.4	11	—	0.3	—	—
45	1991-11-15	22:37	X1.5	3B	S13W19	4	1.5	20	0.28	1.1	0.59	—
46	1992-02-14	23:07	M7.0	2B	S12E02	1	1.0	12	—	—	—	—
47	1992-02-27	08:08	C2.6	SF	N03W05	0.6	1.2	20	—	—	—	—
48	1992-06-28	04:54	X1.8	SF	N11W90	14	1.3	10	0.22	14	1.8	—
49	1994-01-16	23:17	M6.1	1N	N07E71	9	1.2	35	—	—	—	—
50[2]	1997-11-04	05:57	X2.1	2B	S14W33	3	1.0	18	2.3	72	1.5	—
51	1998-08-08	03:15	M3.0	—[‖]	N14E72	0.7	2.0	24	—	—	—	—
52	1998-08-22	00:01	M9.0	2B	N42E51	6	1.0	18	—	2.5	—	—
53[2]	1998-11-22	06:38	X3.7	1N	S27W82	7	6.7	20	0.22	4	—	—

Table 1. (Continued)

No.^{Q*}	Date	T_{peak}	Flare			Microwave burst			Protons near Earth			
			GOES	Hα	Position	Δt_{35} (min)	F_{max} (10^3 sfu)	f_{peak} (GHz)	J_{100} (pfu)	J_{10} (pfu)	δ_p	GLE (%)
1	2	3	4	5	6	7	8	9	10	11	12	13
54[1]	1999-08-20	23:06	M9.8	1N	S23E60	1	3.0	29	—	—	—	—
55[2]	1999-12-28	00:43	M4.5	2B	N23W47	2	2.2	14	0.1	0.5	0.69	—
56[1]	2000-09-30	23:19	X1.2	SF	N09W75	4	5.2	29	—	—	—	—
57[2]	2000-11-24	04:59	X2.0	3B	N19W05	2	9.3	32	0.58	8	1.13	—
58[2]	2001-03-10	04:03	M6.7	1B	N26W42	1	1.6	24	—	0.2	—	—
59[1]	2001-04-03	03:36	X1.2	1N	S21E71	31	2.9	11	0.1	100	3	—
60[2]	2001-04-10	05:32	X2.3	3B	S24W05	30	2.9	9	0.47	355	2.87	—
61[0]	2001-10-12	03:23	C7.6	SF	N16E70	1	1.3	40	—	—	—	—
62[1]	2001-10-25	05:18	C5.2	SF	S19W17	1	1.2	25	—	1	—	—
63[2]	2002-02-20	06:11	M5.1	1N	N13W68	5	1.5	27	0.1	—	—	—
64[1]	2002-07-18	03:32	M2.2	SB	N19W27	2	1.4	20	—	—	—	—
65[1]	2002-08-20	01:49	M5.0	SF	S08W34	0.5	1.8	40	0.07	—	—	—
66[2]	2002-08-21	01:38	M1.4	SF	S10W47	1	1.3	26	—	—	—	—
67[2]	2002-08-21	05:31	X1.0	1B	S09W50	0.7	1.4	27	—	—	—	—
68[1]	2003-04-26	00:55	M2.1	SF	N20W65	2	2.2	30	—	—	—	—
69[1]	2003-04-26	03:03	M2.1	SN	N20W69	0.3	2.4	30	—	—	—	—
70[2]	2003-05-28	00:26	X3.6	1B	S08W22	14	3.4	16	0.15	121	2.9	—
71[2]	2003-05-29	01:01	X1.2	2B	S07W31	12	1.2	14	—	—	—	—
72[2]	2003-05-31	02:21	M9.3	2B	S06W60	8	1.7	15	0.8	27	1.53	
73[1]	2003-06-15	23:44	X1.3	SF	S07E80	8	1.9	11	—	0.3	—	—
74[1]	2003-06-17	22:53	M6.8	—‖	S08E58	23	1.8	30	0.02	16	2.9	—
75[1]	2003-10-24	02:46	M7.6	1N	S19E72	32	3.9	30	—	—	—	—
76[1]	2003-10-26	06:14	X1.2	3B	S17E42	62	3.6	17	—	—	—	—
77	2004-01-06	06:22	M5.8	—‖	N05E89	8	1.0	12	—	—	—	—
78[1]	2004-01-07	03:59	M4.5	2N	N02E82	9	1.8	40	—	—	—	—
79[0]	2004-07-16	02:03	X1.3	—‖	S10E39	5	1.5	20	—	—	—	—
80[1]	2004-08-14	05:43	M7.4	2N	S12W29	7	1.1	20	—	—	—	—
81[2]	2004-10-30	06:14	M4.2	SF	N13W21	7	1.3	20	0.04	0.9	1.35	—
82[1]	2004-11-03	03:30	M1.6	1N	N07E46	10	1.1	9	—	0.4	—	—
83[1]	2005-01-01	00:29	X1.7	—‖	N04E35	6	1.7	15	—	—	—	—
84[0]	2005-01-15	00:41	X1.2	1B	N13E05	6	3.3	20	—	—	—	—
85[1]	2005-07-30	06:25	X1.3	2B	N11E58	27	1.1	10	—	—	—	—
86[1]	2005-08-25	04:38	M6.4	1N	N08E82	5	4.3	26	—	—	—	—
87[0]	2005-09-13	23:21	X1.7	1B	S11E10	6	5.0	36	—	90	—	—
88[1]	2005-09-17	06:05	M9.8	2N	S11W41	6	1.3	25	—	1.4	—	—
89[2]	2011-08-04	03:57	M9.3	2B	N16W49	11	1.4	11	1.5	77	1.71	—
90[2]	2011-08-09	08:05	X6.9	2B	N17W83	6	1.0	14	2.5	22	0.94	—
91[2]	2012-01-23	03:59	M8.7	2B	N29W36	39	2.0	4	2.3	2700	3.07	—
mM events with strong proton fluxes ($J_{100} > 10$ pfu, $10^2 < F_{35} < 10^3$ sfu)												
92[2]	2000-11-08	23:28	M7.8	1N	N10W75	53	0.14	2.8	320	14000	1.64	—
93[2]	2001-12-26	05:40	M7.1	1B	N08W54	26	0.78	6.9	47	700	1.17	13
94[2]	2002-04-21	01:15	X1.5	1F	S14W84	83	$\sim$0.4†,‡	5	20	2000	2.00	—
95[2]	2012-05-17	01:47	M5.1	1F	N09W74	17	0.2	10	18	230	1.11	16
mO backside events with strong proton fluxes ($J_{100} > 10$ pfu)												
96	1990-05-28	04:33‖	—	—	N36W120	8	0.1	1.4	43	430	1.00	6
97	2001-04-18	02:15‖	C2.2	—	S20W115	4	—	—	12	230	1.28	26
98	2001-08-15	—‖	—	—	W > 120	—	—	—	27	470	1.24	—

* The superscript, Q, specifies the qualifier of the event defined as follows: Q0–East event, no CME, no type II burst; Q2–West event with a CME and a type II burst; Q1–For all other events.

† Interpolated from data at 17 and 80 GHz.

‡ Estimated from NoRH data.

§ Estimated from lower-frequency data.

‖ Uncertain.

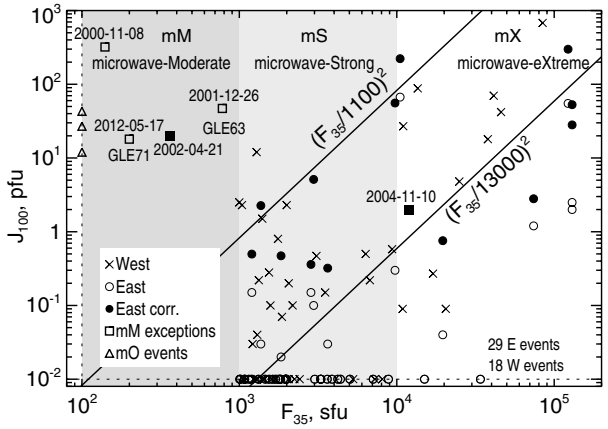

Fig. 1. Fluxes of > 100 MeV protons vs. radio fluxes at 35 GHz. The filled squares denote the events with increased uncertainties of 35 GHz fluxes. The black solid lines are arbitrarily chosen to verify a direct relation between the observed F_{35} and J_{100}.

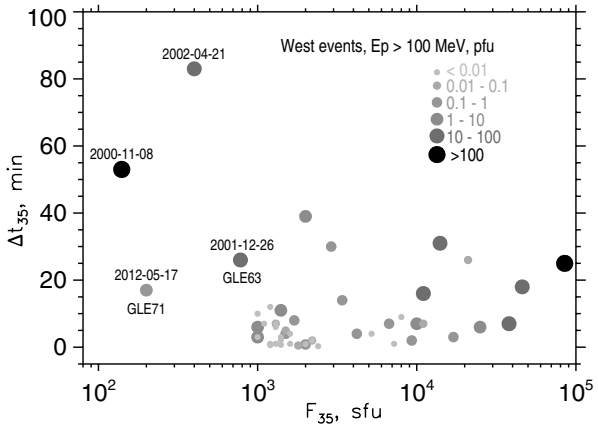

Fig. 2. Distribution of > 100 Mev SEP events associated with the west source regions vs. peak fluxes and durations of 35 GHz bursts. The peak proton fluxes are coded by the size and color of the filled circles. The dates of the four mM exceptions are specified.

events with microwave fluxes $F_{35} < 100$ sfu (triangles) are shown at the vertical dotted line corresponding to 100 sfu.

The SEP fluxes, whose sources have eastern locations (empty circles), are known to be reduced due to the bend of the Parker spiral deflecting charged particles away from the Earth. We have additionally plotted these events with filled circles by applying an empirical correction for the dependence of $\exp^{-[(\lambda-54)/63]^2}$ on the longitude λ (A. Belov 2012 private communication) to partially compensate for the reduction. The plot in figure 1 suggests that this correction might probably be somewhat overestimated.

The following groups of events are distinct in figure 1:

1. Events exhibiting a direct tendency between F_{35} and J_{100}, which occupy a wide band from the lower-left corner to the upper-right one ('main sequence').
2. Strong bursts at 35 GHz without SEPs, schematically shown along the lower horizontal dotted line.
3. Three big SEP events associated with backside sources (mO), schematically shown along the left vertical dotted line.
4. Four exceptional mM events with large proton fluxes (squares in the upper-left region).

Group 1. Events of the 'main sequence' show a general correspondence between the proton fluxes and the F_{35} fluxes, being mostly within the band bounded with rather arbitrary lines of $(F_{35}/1100)^2$ and $(F_{35}/13000)^2$, which reflect a direct flare–SEP relation. The scatter is large for obvious reasons. For example, flare-accelerated protons are affected by the escape conditions from the active regions; shock-accelerated protons are influenced by the plenitude of a seed population; and all depend on the Sun–Earth connections.

Group 2. Two well-known reasons can account for the absence of SEPs in these events. Those are the east location, which was already mentioned, and a short duration. Poor proton production in short-duration 'impulsive' events established a long time ago is usually interpreted by different acceleration mechanisms, in contrast to 'gradual' events (see, e.g., Croom 1971; Cliver et al. 1989; Reames 2009, 2013, and references therein). Possible additional reasons for the differences between these two categories are discussed in section 4. To make the situation with the durations in the considered set clearer, we plotted the west events on the F_{35}–Δt_{35} plane in figure 2 while coding their SEP importance by different size and color of the filled circles. Indeed, low SEP fluxes were observed in short-duration events concentrated at the bottom part of the plot. We remind that the burst durations at 35 GHz are generally shorter than for longer-wave bursts, and always shorter than in soft X-rays, which are usually considered.

Group 3. No conclusion can be drawn for the three mO backside events due to a lack of information about microwave sources occulted by the limb. The soft X-ray and microwave fluxes ascribed to some of these events might be inadequate.

Group 4. The four mM exceptions with moderate microwave flux and incomparably strong SEP events are located high above the 'main sequence.' Two of these events produced GLEs: 2001 December 26 (GLE63) and the recent event of 2012 May 17 (GLE71). Two remaining events, 2000 November 8 and 2002 April 21, are also well known. The SEP spectra in these events $\delta_{\rm p} \leq 2$ were relatively hard, with $\delta_{\rm p} < 1.2$ in two GLE events, being atypical of non-flare-related filament eruptions, where $\delta_{\rm p} \sim 3$ (Chertok et al. 2009). There are no obvious indications of reasons for the exceptional characteristics of these events. The significance of group 4 is supported by the absence of $J_{100} > 10$ pfu enhancements among the mS events.

3.2. *Relation to SEP Spectra*

The SEP spectra were relatively hard, $\delta_{\rm p} \leq 2$, in most west events with a high $f_{\rm peak} > 20$ GHz. There is a weak tendency of hardening the proton spectra (decrease of $\delta_{\rm p}$) with an increase of the microwave peak frequency, $f_{\rm peak}$. This tendency is consistent with the conclusions of Chertok et al. (2009). The statistics of SEP events with known $\delta_{\rm p}$ in table 1 is relatively poor to figure out this tendency with confidence. We therefore involve additional information from

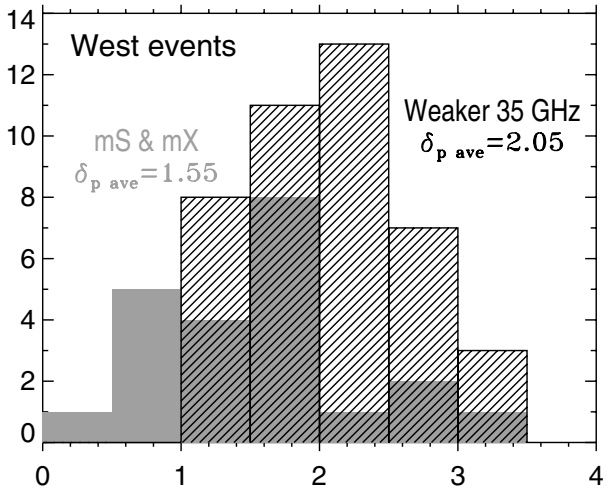

Fig. 3. Histograms of the proton energy index, $\delta_{\rm p}$, for SEP events with strong NoRP 35 GHz bursts (mS and mX, shaded) and for SEP events with weaker RSTN bursts (line-filled).

Chertok et al. (2009) concerning SEP events and radio bursts recorded with the USAF RSTN network during 1988–2006.[3]

To minimize the influence of the heliolongitude on the SEP spectrum, only those events associated with west solar sources are analyzed. We compare two subsets of SEP events: (i) SEP events with corresponding NoRP mX and mS bursts ($F_{35} > 10^3$ sfu) from table 1, and (ii) events without strong bursts at 35 GHz selected from Chertok et al. (2009). Subset (ii) contains only events in which $F_{35} < 10^3$ sfu, judging from the lower-frequency RSTN data.

The distribution of $\delta_{\rm p}$ in the two subsets is shown in figure 3. The shaded histogram presents SEP events with a certain $\delta_{\rm p}$ corresponding to NoRP mX and mS bursts from west solar sources. These are events Nos. 2, 9, 11, 12, 14, 15, 16, 17, 19, 34, 45, 48, 50, 55, 57, 60, 70, 72, 81, 89, 90, and 91 (totally 22 events). The line-filled histogram presents SEP events (also from west solar sources), which were not preceded by strong bursts at 35 GHz (totally 42 events, including the four exceptional mM events, Nos. 92–95).

Indeed, the SEP events after strong 35 GHz bursts had predominantly harder spectra with an average $\overline{\delta_{\rm p}} = 1.55$. The histogram for the second subset with an average $\overline{\delta_{\rm p}} = 2.05$ is apparently shifted right. The exclusion of the four exceptional mM events (Nos. 92–95, $\delta_{\rm p} = 1.11$–2.00, squares in the upper left region of figure 1) from the histogram increases $\overline{\delta_{\rm p}}$ to 2.11 in the second subset.

4. Discussion

The characteristics of the mX events, whose microwave peak frequencies reach very high values (32 GHz on average), suggest flaring above the sunspot umbrae, where the strongest magnetic fields are reached. This conclusion follows from the properties of gyrosynchrotron emission (Dulk & Marsh 1982; Stahli et al. 1989; Krucker et al. 2013), as the next section confirms. The strong dependence of the energy release rate on the magnetic field strength is expected from the standard flare model, as Asai et al. (2002, 2004) have shown. Grechnev et al. (2008) and Kundu et al. (2009) also demonstrated extreme parameters of sunspot-associated flares, such as strong hard X-ray and gamma-ray emissions and high SEP productivity.

Figure 4 confirms this assumption for three extreme events: 2005 January 20 (a, b; X7.1, No. 16, GLE69), 2006 December 13 (c, d; X3.4, No. 17, GLE70), and 2012 March 07 (e, f; X5.4, No. 18). The ribbons crossed the sunspot umbrae also in a series of big white-light flares, which occurred on 1991 June 4, 9, and 11 (Sakurai et al. 1992; events Nos. 6, 8, and 9 in table 1). Flaring above the sunspot umbrae seems to be typical of mX and some mS events, indeed.

4.1. Well-Sampled Event of 2001 August 25

To provide further verification of the assumption concerning the relation of strong high-frequency bursts with flaring in strong magnetic fields above the sunspot umbrae, we briefly consider an extreme white-light flare of 2001 August 25 (X5.3/3B, S17E34). This flare (Metcalf et al. 2003) was responsible for a big neutron event, extreme hard X-ray and gamma-ray emissions (Watanabe et al. 2003; Kuznetsov et al. 2006; Livshits et al. 2006), and a fast CME. The SEP event was not pronounced at Earth due to the east location of the solar region. The event occurred during the nighttime in Nobeyama; nevertheless, we used NoRH data to estimate a probable magnetic field strength in the flaring region.

This flare was chosen for a unique coverage of its spectrum at 1–18 GHz (Owens Valley Solar Array, OVSA), at 89.4 GHz (the nulling interferometer at Bern University), and at 212 and 405 GHz (Solar Submillimeter-wave Telescope, SST). The radio measurements from microwaves up to submillimeters were addressed by Raulin et al. (2004), who concluded that the gyrosynchrotron emission up to $\sim 10^5$ sfu was produced by electrons radiating in a 1000–1100 G region, because '*magnetic fields higher than 1100 G should be excluded, since they produce a peak frequency at or above 90 GHz, which was not observed*.' The authors mentioned the possibility of an inhomogeneous source, but their model did not include it. Krucker et al. (2013) confirmed the gyrosynchrotron mechanism of the submillimeter emission in this event.

Figure 5 shows TRACE white-light images of the active region before the flare (left) and the flare configuration near the peak of the event (right). The east flare ribbon intruded far into the umbrae of the east S-polarity sunspot. The west ribbon covered the edge of the west N-polarity sunspot's umbra. The black contours present hard X-ray sources, whose images we have produced from Yohkoh/HXT (Hard X-ray Telescope) data in the 33–53 keV M2 channel (Kosugi et al. 1991).

The flare configuration with the ribbons above the umbrae corresponds to our expectations. Although Raulin et al. (2004) inferred strong magnetic fields in the gyrosynchrotron source, we reconsider the conclusion of the authors about the field strength in this extreme event by using a simple model of an inhomogeneous gyrosynchrotron source, described by Kundu et al. (2009).

The first point in question is a probable magnetic field

[3] These data are available at ⟨http://www.izmiran.ru/∼ichertok/SEPs_radio/Table.html⟩.

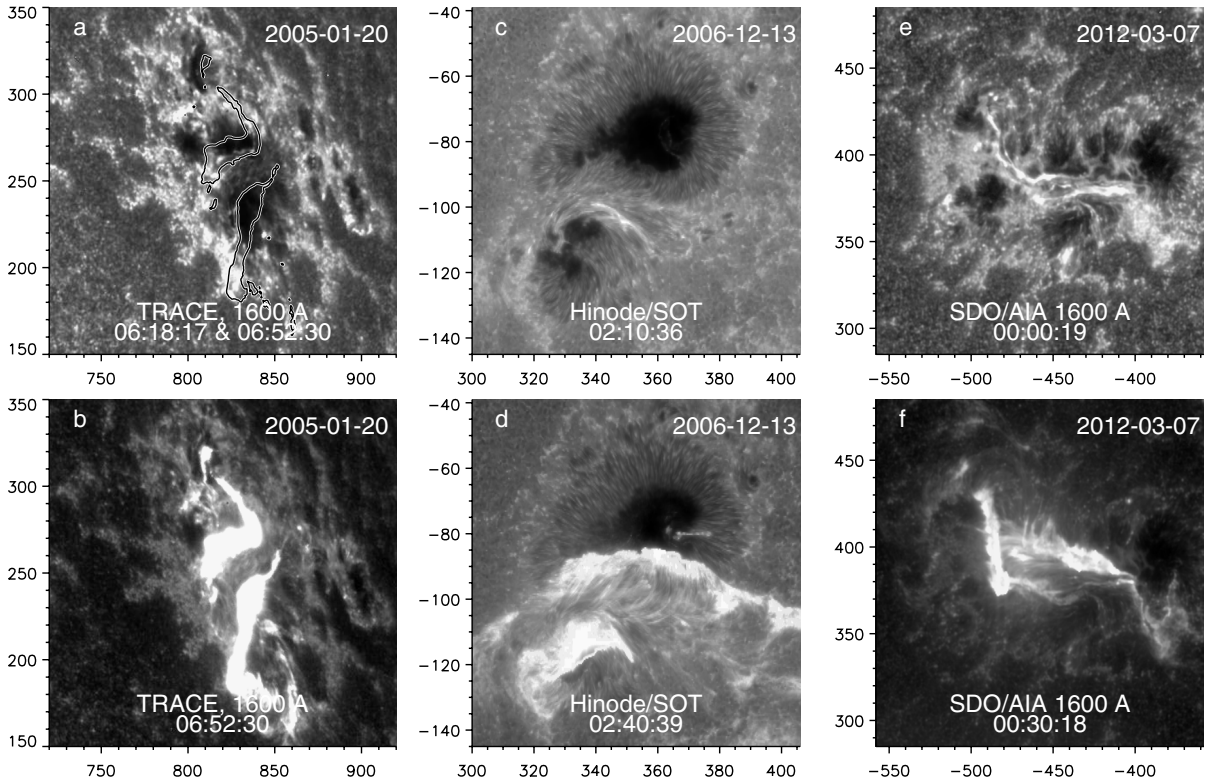

Fig. 4. Three sunspot-associated flares on 2005 January 20 (a, b), on 2006 December 13 (c, d), and on 2012 March 07 (e, f). Top: before the flare, bottom: during the flare. The contours overlayed on the image in panel (a) outline the ribbons visible in panel (b). The axes show hereafter arc seconds from the solar disk center.

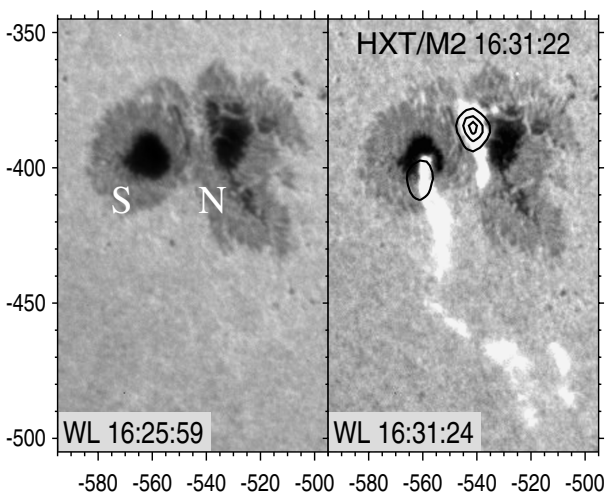

Fig. 5. Flare configuration in the 2001 August 25 extreme event. The gray-scale background presents white light images (TRACE) before the flare (left) and during the flare peak (right). Contours in the right panel present HXR (hard X-ray) sources (Yohkoh/HXT/M2, 33–53 keV). The contour levels are [0.2, 0.5, 0.8] of the maximum value. The magnetic polarities of the sunspots are indicated in the left panel.

strength in the corona, where the flare source was located. To estimate it, we analyzed the maximum field strengths in both sunspots from a one-week-long set of 96-min MDI magnetograms, and referred them to NoRH observations. The secant correction was applied to the magnetograms (the 'zradialize' SolarSoft routine). The magnetograms suffer from 'high-field saturation,' especially in the east sunspot of the S-polarity. Figure 6 presents the maximum field strengths measured in the positive west sunspot (top) and the negative east sunspot (bottom) with small circles. The 'saturation' is especially pronounced in the larger scatter of the bottom plot.

The gray curves present a boxcar smoothing of the measured points over 15 neighbors. The plots show an unrealistic rise of the magnetic field strength near the limb before August 23–24, suggestive of an excessive secant correction. We consider the shaded region to be spurious.

The upper black curves approximately enveloping the measured points were computed by magnifying the gray curves by factors of 1.025 for the N-polarity sunspot and 1.060 for the S-polarity sunspot. They present the evolution of a probable maximum field at the photospheric level, which might still be underestimated. However, the magnetic field strength in the corona is important. To estimate it, we note that NoRH observations at 17 GHz on August 27–29 reveal a sunspot-associated source above the east sunspot with a brightness temperature of 0.2–0.5 MK and a degree of polarization $> 50\%$. These properties are typical of the gyroresonance emission, which occurs in sunspot-associated sources at 17 GHz at the third harmonic of the gyrofrequency, i.e., in magnetic fields of ≈ 2000 G (Vourlidas et al. 2006). The lower curves in figure 6 are referred to this estimate, and calculated as the upper envelopes reduced by a factor of 0.53. We obtained probable magnetic

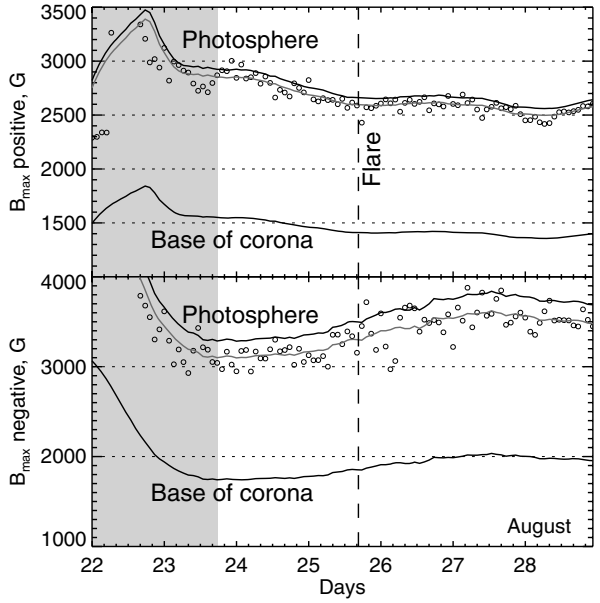

Fig. 6. Estimation of the probable magnetic field strength from one-week-long MDI magnetograms and NoRH observations. The circles present the maximum field strength in each sunspot measured from radialized 96-min magnetograms (top N-polarity, bottom S-polarity). The gray curves show their smoothing. The upper black envelopes of the measured points present evolution of the probable maximum field at the photosphere. The reduced lower black curves correspond to the base of the corona. The radialization in the shaded interval is most likely unrealistic.

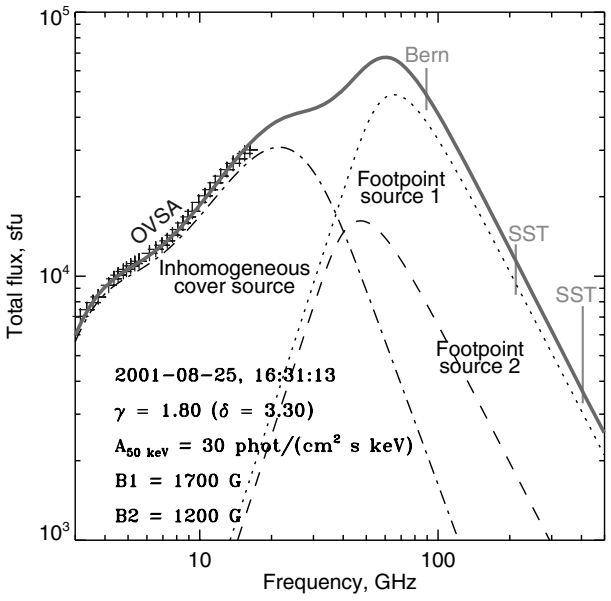

Fig. 7. Gyrosynchrotron spectrum of the 2001 August 25 extreme flare. The symbols present the observations of OVSA (crosses), Bern, and SST (gray bars). The thick curve was calculated from the model. The dotted and dashed curves show the spectra of two footpoint kernel sources. The dash-dotted curve presents the inhomogeneous cover source in the top part of the magnetic configuration.

field strengths at the base of the corona during the flare (the vertical dashed line) of about +1400 G in the west sunspot and −1800 G in the east sunspot.

Figure 7 presents with symbols the spectrum observed close to the flare peak (from Raulin et al. 2004) along with the model one presented with the thick line. The three-component model (Kundu et al. 2009) simulates emission from two footpoint sources (dotted and dashed) visible through an inhomogeneous frequency-dependent cover source (dash-dotted; see Bastian et al. 1998) based on the expressions from Dulk and Marsh (1982) and White et al. (2011). The parameters of the HXR spectrum were evaluated by V. Kurt from data of CORONAS-F/SONG (Kuznetsov et al. 2011), Yohkoh/GRS and HXT (Yoshimori et al. 1991; Kosugi et al. 1991): $\gamma = 2.0$, $A_{50\,\mathrm{keV}} = 30\,\mathrm{photons\,cm^{-2}\,s^{-1}\,keV^{-1}}$. A small difference between the index, $\gamma = 1.8$, used in the model and the actual $\gamma = 2.0$ could be due to the spectral hardening of trapped electrons (Melnikov & Magun 1998; Silva et al. 2000; Kundu et al. 2009). The size of each source was estimated from the HXT/M2 image in figure 5. The magnetic field strengths in the sources were taken to be −1700 G and +1200 G.

The model correctly reproduces the main features of the observed spectrum. Invoking the inhomogeneous source removes the limitation of B ≤ 1100 G, which restrained considerations of Raulin et al. (2004); the magnetic field in the source region could be considerably stronger than the authors concluded. The very strong magnetic field in the flare region determined the extreme properties of this big flare, indeed. This example also shows that the turnover frequency of the gyrosynchrotron spectrum can be displaced left due to the contribution of a large inhomogeneous cover source, thus affecting column 9 in table 1. The displacement can be large, and hide an indication of strong fields in the lowest part of the flare configuration (White et al. 2003; Kundu et al. 2009).

4.2. Exceptional mM Events

The four exceptional mM events from group 4 (squares in the upper left part of figure 1) look challenging: large proton enhancements, $J_{100} > 10$ pfu, occurred in association with moderate bursts, in which $F_{35} < 1000$ sfu. The peak frequencies of the microwave spectra in these events were below 10 GHz. The 'Big Flare Syndrome' and the presumable exclusive responsibility of the shock-acceleration do not clarify the situation: while a fast CME and strong shock are expected after a big flare, such expectations from a moderate flare seem unlikely (see section 1).

The relation between the microwave fluxes from the four exceptional events and their proton productivity appears to be distorted for some reasons. The first possibility is prompted by the locations of the mM exceptions in figure 1, close to the occulted mO events, i.e., possible contributions from nearly simultaneous backside events.

The solar source of the 2000 November 8 event (No. 92 in table 1) is ascribed to an M7.8/1N flare in active region (AR) 9212 (Kurt et al. 2004) or AR 9213 (Nitta et al. 2003). A related CME had an average speed of 1738 km s^{-1} and an extrapolated onset time of ≈ 22:48 at 1 $R_\odot$ (CME catalog). A type II burst started by 22:50 (HiRAS spectrometer), close to the CME onset, but well before a weak microwave burst, which started after 23:04. According to Zhang et al. (2001) and

Temmer et al. (2008, 2010), the microwave burst is expected to be ~ 15 min earlier. Nitta et al. (2003) proposed that '*the associated SEP event appears to have originated in the non-active region eruption rather than the M7.7 flare, although the entire complex of minor active regions was probably involved at some level*'. However, such a fast CME is not expected from a non-active region eruption. A proton index of $\delta_{\rm p} = 1.64$ is atypically hard of SEP events after such eruptions, in which usually $\delta_{\rm p} > 2$ (Chertok et al. 2009). These facts hint at a possible implication of a backside eruption.

The 2001 December 26 event (No. 93) also looks strange. The source of the SEP event is ascribed to the M7.1/1B flare in AR 9742, N08W54 (Kurt et al. 2004; Cliver 2006). Identification of the solar source is hampered by a gap in EIT observations between 04:47 and 05:22. The situation on the Sun with several minor active regions and post-eruption manifestations look similar to the preceding event. The major role of a non-active region eruption for the SEP event with $\delta_{\rm p} = 1.17$ responsible for GLE63 looks still more doubtful than for the 2000 November 8 event. The CME (1446 km s^{-1}) and the main microwave burst started at about 05:06, while the type II burst started by 04:50 (HiRAS). The soft X-ray emission in this event rose much longer than in all other GLE events of solar cycle 23 (Aschwanden 2012), while the rise phase roughly displays the CME velocity (Zhang et al. 2001). A strong shock wave is not expected from a gradually expanding CME. Possibly, the M7.1 flare was preceded by a stronger backside event.

The microwave burst in the 2002 April 21 event (No. 94) looks too moderate in comparison with the big SEP event, the X1.2 flare, and the fast CME (2393 km s^{-1}). The near-limb location of the flare site (S14W84) implies complications like partial occultation of the flaring region or some kind of absorption of the microwave emission, suggested by its atypically flat spectrum. The presence of three major peaks in the microwave time profile, the first of which corresponded to the CME onset time, suggests more than one eruption and additional features of this event, such as the merger of two to three shock waves into a stronger one.

The 2012 May 17 event (No. 95) was responsible for GLE71. The M5.1 GOES importance was the lowest one among all GLEs of the solar cycles 22–24 (Cliver 2006). The CME had an average speed of 1582 km s^{-1}. A flare ribbon crossed the sunspot umbra. STEREO-A did not show any candidate for a stronger event behind the west limb. Some kind of absorption of the microwave emission is not excluded (the spectrum was also flat), but the moderate GOES importance does not support an underestimation of the flare emission. Like the preceding event, the microwave time profile had three peaks, the first of which corresponded to the CME onset. The moderate GOES importance and the microwave flux suggest the possibility of the escape of an unusually large fraction of accelerated particles, including electrons, into interplanetary space. Analysis of this event is anticipated.

Thus, possible causes of the mM exceptions can be different. These events deserve attention and further investigation. The group of such events can actually be larger: we did not analyze SEP events with $J_{100} < 10$ pfu, or those occurring beyond the observational daytime in Nobeyama.

4.3. Account of Properties of Events

Subsection 3.1 and figure 2 confirm the well-known fact of a poorer proton production of short-duration events. The conclusion concerning the distinction of SEP events into 'gradual' and 'impulsive' categories (with an intermediate 'mixed' group) has been drawn from observations, which were related to solar sources indirectly. The duration criterion referring to microwave or soft X-ray bursts (see, e.g., Cliver et al. 1989) also considers indirect outer manifestations of solar events.

As shown in section 1, the scenario of a solar event offers very different opportunities for the development of a shock wave and the escape of protons from an active region. In a typical powerful CME-productive event, a sharp eruption excites a shock wave capable of particle acceleration, and the CME lift-off makes possible the escape of most flare-accelerated particles trapped in the CME's flux rope. An opposite extremity of a confined flare does not produce a shock wave, while escape is possible for those accelerated particles, which are brought by drifts and diffusion to open magnetic fields permanently existing in active regions. The bulk of accelerated protons remains trapped. By chance, we know that events Nos. 87 and 88 in 2005 September were most likely to be confined flares. Their durations were indeed short. On the other hand, the durations of the four mM exceptions were considerable (figure 2).

Probably, failed eruptions, like the event presented by Ji et al. (2003), also do not produce shock waves, nor favor particle escape. There may be confined eruptions that excite shock waves, but do not produce CMEs. Jet-like eruptions seem to favor the escape of flare-accelerated particles, while related shock waves probably rather rapidly dampen due to the absence of significant energy supply from any trailing ejecta. The variety of types of flares and eruptions might respond in their SEP outcome. The most apparent, well-known indication of a shock wave, is a type II burst (although the absence of a type II emission does not guarantee the absence of a shock), and an indication of an opening magnetic configuration is a CME. We have found information about CMEs for 52 events, which occurred since 1996 (after the launch of SOHO) through 2012. It is presented by the qualifier Q0, Q1, Q2 as a superscript in column 1 of table 1, described in subsection 2.2. These 52 events are plotted in figure 8. The longitudinal correction was applied for the east events. The mM exceptions are qualified as Q2. The backside mO events are not shown due to the absence of any relevant information. Figure 8 shows the following:

1. The majority of west events with both CMEs and type II bursts (Q2 events) belongs to the 'main sequence.' Three non-proton-productive Q2 events are nevertheless located close to the 'main sequence.'
2. No near-Earth fluxes of >100 MeV protons were detected after east events, which were associated with neither CME nor type II burst. These are five Q0 events.
3. Most remaining events (17 Q1 events) did not produce near-Earth protons with energies >100 MeV. Four Q1 events belong to the main sequence.

A simple criterion follows from this distribution: if an

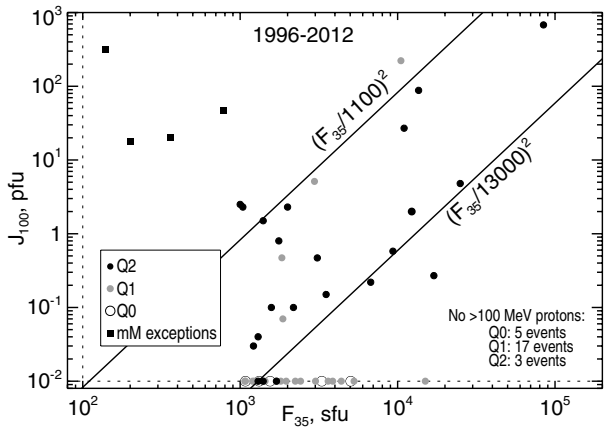

Fig. 8. Distribution of NoRP events, which occurred in 1996–2012, in the same format as figure 1, i.e., fluxes of > 100 MeV protons vs. radio fluxes at 35 GHz. The symbols denote the qualifiers of the events according to the legend in the frame. The black solid lines delimit the 'main sequence'.

event has a west location and produces both CME and type II burst, then the near-Earth flux of > 100 MeV protons expected from this event should be most likely between $(F_{35}/1100)^2$ and $(F_{35}/13000)^2$ pfu. This criterion can be possibly used as a tentative basis for a future prompt diagnostics of proton events.

5. Conclusion

Recent observations and their studies have revealed still closer relations between solar eruptions, flares, shock waves, and CMEs, than previously assumed. This circumstance provides a basis to expect a closer correspondence between parameters of near-Earth proton enhancements and microwave bursts than the 'Big Flare Syndrome' can predict. This expectation has been mainly confirmed in the present brief analysis of relations between about one hundred of strong microwave bursts recorded in 1990–2012 with NoRP at 35 GHz and near-Earth proton fluxes.

There is a scattered general correspondence between the peak flux density at 35 GHz and the peak flux of > 100 MeV protons, $J_{100} \approx (F_{35}/3800)^2$. In accordance with well-known patterns, events with $F_{35} < 10^4$ sfu in far-east active regions as well as events with short-duration bursts have a reduced proton outcome up to zero. On the other hand, most west events associated with intense 35 GHz bursts, CMEs, and type II bursts produce near-Earth fluxes of > 100 MeV protons between $(F_{35}/1100)^2$ and $(F_{35}/13000)^2$ pfu. Overall, extreme long-duration bursts at 35 GHz ($F_{35} > 10^4$ sfu) indicate large proton enhancements with predominantly hard energy spectra, including GLEs. Large SEP events are possible, even with an eastern location of a solar source region, if the 35 GHz burst is especially intense.

A morphological manifestation of a high-intensity burst at 35 GHz is a flare occurring above the sunspot umbra. This is a different indication of a possible SEP event. Thus, strong high-frequency bursts or/and flare ribbons crossing the sunspot umbrae can be employed to promptest alert of SEP events. However, in the case of a backside flare, its microwave emission is occulted for radiometers at Earth, while energetic particles propagating along the Parker spiral can reach Earth.

Another limitation of diagnostic opportunities of microwave observations is offered by challenging big SEP enhancements, which rather rarely occur in association with moderate microwave bursts. Such events deserve special attention and need investigating. Case studies of various events can significantly contribute to a better understanding of their SEP productivity and related conditions.

While some questions remain unanswered, it is clear that NoRP and NoRH observations are highly important in further investigating the SEP problem.

We thank V. Kurt, A. Belov, A. Uralov, H. Nakajima, B. Yushkov, K.-L. Klein, A. Tylka, S. White, Y. Kubo, N. Nitta, and S. Kalashnikov for fruitful discussions and assistance. We thank an anonymous referee for useful suggestions. We are grateful to the instrumental teams operating the Nobeyama solar facilities and GOES satellites. Data on CMEs have been taken from the on-line CME catalog generated and maintained at the CDAW Data Center by NASA and the Catholic University of America in cooperation with the Naval Research Laboratory. SOHO is a project of international cooperation between ESA and NASA.

This study was supported by the Russian Foundation of Basic Research under grants 11-02-00757 and 12-02-00037, the Program of the RAS Presidium No. 22, and the Russian Ministry of Education and Science under projects 8407 and 14.518.11.7047. N.M. was sponsored by a Marie Curie International Research Staff Exchange Scheme Fellowship within the 7th European Community Framework Programme.

References

Ackermann, M., et al. 2012, ApJ, 745, 144
Afanasyev, A. N., & Uralov, A. M. 2011, Sol. Phys., 273, 479
Akinian, S. T., Alibegov, M. M., Kozlovskii, V. D., & Chertok, I. M. 1978, Geomagn. Aeron., 18, 410
Asai, A., Masuda, S., Yokoyama, T., Shimojo, M., Isobe, H., Kurokawa, H., & Shibata, K. 2002, ApJ, 578, L91
Asai, A., Yokoyama, T., Shimojo, M., Masuda, S., Kurokawa, H., & Shibata, K. 2004, ApJ, 611, 557
Aschwanden, M. J. 2012, Space Sci. Rev., 171, 3
Bastian T. S., Benz A. O., & Gary D. E. 1998, ARA&A, 36, 131
Chertok I. M., Grechnev V. V., & Meshalkina N. S. 2009, Astron. Rep., 53, 1059
Chupp, E. L., & Ryan, J. M. 2009, Res. Astron. Astrophys., 9, 11
Cliver, E. W. 2006, ApJ, 639, 1206
Cliver, E. W., Forrest, D. J., Cane, H. V., Reames, D. V., McGuire, R. E., von Rosenvinge, T. T., Kane, S. R., & MacDowall, R. J. 1989, ApJ, 343, 953
Cliver, E. W., Kahler, S. W., Shea, M. A., & Smart, D. F. 1982, ApJ, 260, 362
Croom, D. L. 1971, Sol. Phys., 19, 152

Dulk, G. A., & Marsh, K. A. 1982, ApJ, 259, 350
Forrest, D. J., Vestrand, W. T., Chupp, E. L., Rieger, E., Cooper, J., & Share, G. H. 1986, Adv. Space Res., 6, 115
Gopalswamy, N., Xie, H., Yashiro, S., Akiyama, S., Mäkelä, P., & Usoskin, I. G. 2012, Space Sci. Rev., 171, 23
Grechnev, V. V., et al. 2008, Sol. Phys., 252, 149
Grechnev, V. V., Afanasyev, A. N., Uralov, A. M., Chertok, I. M., Eselevich, M. V., Eselevich, V. G., Rudenko, G. V., & Kubo, Y. 2011b, Sol. Phys., 273, 461
Grechnev, V. V., Uralov, A. M., Chertok, I. M., Kuzmenko, I. V., Afanasyev, A. N., Meshalkina, N. S., Kalashnikov, S. S., & Kubo, Y. 2011a, Sol. Phys., 273, 433
Ji, H., Wang, H., Schmahl, E. J., Moon, Y.-J., & Jiang, Y. 2003, ApJ, 595, L135
Kahler, S. W. 1982, J. Geophys. Res., 87, 3439
Kallenrode, M.-B. 2003, J. Phys. G, 29, 965
Klein, K.-L., & Trottet, G. 2001, Space Sci. Rev., 95, 215
Kosugi, T., et al. 1991, Sol. Phys., 136, 17
Krucker, S., et al. 2013, A&AR, 21, 58
Kundu, M. R., Grechnev, V. V., White, S. M., Schmahl, E. J., Meshalkina, N. S., & Kashapova, L. K. 2009, Sol. Phys., 260, 135
Kurt, V., Belov, A., Mavromichalaki, H., & Gerontidou, M. 2004, Ann. Geophys., 22, 2255
Kurt, V., Yushkov, B., Belov, A., Chertok, I., & Grechnev, V. 2013, J. Phys. Conf. Ser., 409, 012151
Kuznetsov, S. N., Kurt, V. G., Myagkova, I. N., Yushkov, B. Y., & Kudela, K. 2006, Sol. Syst. Res., 40, 104
Kuznetsov, S. N., Kurt, V. G., Yushkov, B. Y., Kudela, K., & Galkin, V. I. 2011, Sol. Phys., 268, 175
Lin, R. P., et al. 2002, Sol. Phys., 210, 3
Livshits, M. A., Chernetskii, V. A., Bogomolov, A. V., Kuznetsov, S. N., Logachev, Y. I., Myagkova, I. N., Svertilov, S. I., & Yushkov, B. Y. 2006, Sol. Syst. Res., 40, 153
Melnikov, V. F., & Magun, A. 1998, Sol. Phys., 178, 153
Meshalkina, N. S., Uralov, A. M., Grechnev, V. V., Altyntsev, A. T., & Kashapova, L. K. 2009, PASJ, 61, 791
Metcalf, T. R., Alexander, D., Hudson, H. S., & Longcope, D. W. 2003, ApJ, 595, 483
Miklenic, C. H., Veronig, A. M., & Vršnak, B. 2009, A&A, 499, 893
Nakajima, H., et al. 1985, PASJ, 37, 163
Nakajima, H., et al. 1994, Proc. IEEE, 82, 705
Nitta, N. V., Cliver, E. W., & Tylka, A. J. 2003, ApJ, 586, L103
Nitta, N. V., Liu, Y., DeRosa, M. L., & Nightingale, R. W. 2012, Space Sci. Rev., 171, 61
Qiu, J., Hu, Q., Howard, T. A., & Yurchyshyn, V. B. 2007, ApJ, 659, 758
Raulin J. P., Makhmutov, V. S., Kaufmann, P., Pacini, A. A., Lüthi, T., Hudson, H. S., & Gary, D. E. 2004, Sol. Phys., 223, 181
Reames, D. V. 1999, Space Sci. Rev., 90, 413
Reames, D. V. 2009, ApJ, 693, 812
Reames, D. V. 2013, Space Sci. Rev., 175, 53
Sakurai T., et al. 1992, PASJ, 44, L7
Silva, A. V. R., Wang, H., & Gary, D. E. 2000, ApJ, 545, 1116
Stähli, M., Gary, D. E., & Hurford, G. J. 1989, Sol. Phys., 120, 351
Temmer, M., Veronig, A. M., Kontar, E. P., Krucker, S., & Vršnak, B. 2010, ApJ, 712, 1410
Temmer, M., Veronig, A. M., Vršnak, B., Rybák, J., Gömöry, P., Stoiser, S., & Maričić, D. 2008, ApJ, 673, L95
Torii, C., Tsukiji, Y., Kobayashi, S., Yoshimi, N., Tanaka, H., & Enome, S. 1979, Proc. Res. Inst. Atmos., Nagoya Univ., 26, 129
Vilmer, N., MacKinnon, A. L., & Hurford, G. J. 2011, Space Sci. Rev., 159, 167
Vourlidas, A., Gary, D. E., & Shibasaki, K. 2006, PASJ, 58, 11
Vršnak, B., Sudar, D., & Ruždjak, D. 2005, A&A, 435, 1149
Watanabe, K., et al. 2003, Int. Cosmic Ray Conf., 6, 3179
White, S. M., et al. 2011, Space Sci. Rev., 159, 225
White, S. M., Krucker, S., Shibasaki, K., Yokoyama, T., Shimojo, M., & Kundu, M. R. 2003, ApJ, 595, L111
Yashiro, S., Gopalswamy, N., Michalek, G., St. Cyr, O. C., Plunkett, S. P., Rich, N. B., & Howard, R. A. 2004, J. Geophys. Res., 109, A07105
Yoshimori, M., et al. 1991, Sol. Phys., 136, 69
Zhang, J., Dere, K. P., Howard, R. A., Kundu, M. R., & White, S. M. 2001, ApJ, 559, 452